The SCUBA-2 Cosmology Legacy Survey: the clustering of submillimetre galaxies in the UKIDSS UDS field

Aaron Wilkinson,[1]★ Omar Almaini,[1] Chian-Chou Chen,[2,3] Ian Smail,[2,3]
Vinodiran Arumugam,[4,5] Andrew Blain,[6] Edward L. Chapin,[7] Scott C. Chapman,[8]
Christopher J. Conselice,[1] William I. Cowley,[3] James S. Dunlop,[4] Duncan Farrah,[9]
James Geach,[10] William G. Hartley,[11] Rob J. Ivison,[4,5] David T. Maltby,[1]
Michał J. Michałowski,[4] Alice Mortlock,[4] Douglas Scott,[12] Chris Simpson,[13]
James M. Simpson,[4] Paul van der Werf[14] and Vivienne Wild[15]

[1]*School of Department of Physics and Astronomy, University of Nottingham, University Park, Nottingham NG7 2RD, UK*
[2]*Centre for Extragalactic Astronomy, Department of Physics, Durham University, South Road, Durham DH1 3LE, UK*
[3]*Institute for Computational Cosmology, Durham University, South Road, Durham DH1 3LE, UK*
[4]*SUPA (Scottish Universities Physics Alliance), Institute for Astronomy, University of Edinburgh, Royal Observatory, Blackford Hill, Edinburgh EH9 3HJ, UK*
[5]*European Southern Observatory, Karl Schwarzschild Strasse 2, Garching, Germany*
[6]*Department of Physics and Astronomy, University of Leicester, University Road, Leicester LE1 7RH, UK*
[7]*Herzberg Astronomy and Astrophysics, National Research Council Canada, 5071 West Saanich Road, Victoria, BC V9E 2E7, Canada*
[8]*Department of Physics and Atmospheric Science, Dalhousie University, Halifax, NS B3H 3J5, Canada*
[9]*Department of Physics, Virginia Tech, Blacksburg, VA 24061, USA*
[10]*Centre for Astrophysics Research, University of Hertfordshire, College Lane, Hatfield AL10 9AB, UK*
[11]*ETH Zürich, Institut für Astronomie, HIT J 11.3, Wolfgang-Pauli-Strasse 27, Zürich CH-8093, Switzerland*
[12]*Department of Physics and Astronomy, University of British Columbia, 6224 Agricultural Road, Vancouver, BC V6T 1Z1, Canada*
[13]*Astrophysics Research Institute, Liverpool John Moores University, Liverpool Science Park, 146 Brownlow Hill, Liverpool L3 5RF, UK*
[14]*Leiden Observatory, Leiden University, PO Box 9513, NL-2300 RA Leiden, The Netherlands*
[15]*SUPA (Scottish Universities Physics Alliance), School of Physics and Astronomy, University of St Andrews, North Haugh, St Andrews, KY16 9SS, UK*

ABSTRACT

Submillimetre galaxies (SMGs) are among the most luminous dusty galaxies in the Universe, but their true nature remains unclear; are SMGs the progenitors of the massive elliptical galaxies we see in the local Universe, or are they just a short-lived phase among more typical star-forming galaxies? To explore this problem further, we investigate the clustering of SMGs identified in the SCUBA-2 Cosmology Legacy Survey. We use a catalogue of submillimetre (850 μm) source identifications derived using a combination of radio counterparts and colour/infrared selection to analyse a sample of 610 SMG counterparts in the United Kingdom Infrared Telescope (UKIRT) Infrared Deep Survey (UKIDSS) Ultra Deep Survey (UDS), making this the largest high-redshift sample of these galaxies to date. Using angular cross-correlation techniques, we estimate the halo masses for this large sample of SMGs and compare them with passive and star-forming galaxies selected in the same field. We find that SMGs, on average, occupy high-mass dark matter haloes ($M_{halo} > 10^{13}$ M$_\odot$) at redshifts $z > 2.5$, consistent with being the progenitors of massive quiescent galaxies in present-day galaxy clusters. We also find evidence of downsizing, in which SMG activity shifts to lower mass haloes at lower redshifts. In terms of their clustering and halo masses, SMGs appear to be consistent with other star-forming galaxies at a given redshift.

Key words: galaxies: evolution – galaxies: formation – galaxies: high-redshift – galaxies: starburst – large-scale structure of Universe.

★ E-mail: ppxakw@nottingham.ac.uk

1 INTRODUCTION

One key discovery in astronomy to date is the bimodality in the galaxy population, whose origin is still greatly debated. The galaxy population is split into two distinct types both locally and at high redshift: passively evolving red-sequence galaxies and the star-forming blue cloud galaxies (e.g. Strateva et al. 2001; Baldry et al. 2004; Bell et al. 2004; Brammer et al. 2009). The quenching of star formation is believed to cause blue cloud galaxies to migrate to the red sequence. A difference in morphology is also observed. A large fraction of passive galaxies have spheroidal early-type morphologies, in contrast to the star-forming galaxies, which tend to form disc-like structures (Kennicutt 1998).

Various galaxy evolution models have been proposed to explain the morphological transformation and the quenching of star formation in disc galaxies (e.g. Di Matteo, Springel & Hernquist 2005; Croton et al. 2006; Dekel & Birnboim 2006; Hopkins et al. 2006; Somerville et al. 2008; Martig et al. 2009; Trayford et al. 2016). Many of these models invoke major merger events, originally proposed by Toomre (1977). A merging of two or more galaxies can result in a starburst phase in which the merged galaxy experiences a short-lived burst of compact star formation. In the aftermath, stellar or AGN feedback can rapidly expel the remaining gas from the galaxy (e.g. Silk & Rees 1998; Hopkins et al. 2005; Trayford et al. 2016). Alternative models produce compact spheroids using inflow of cold gas, which leads to disc instabilities and contraction (e.g. Dekel, Sari & Ceverino 2009). For a galaxy to remain quenched in its star formation, AGN feedback is required to keep any gas sufficiently heated (Best et al. 2006).

A merger-induced starburst may be responsible for the formation of the most massive ($M_* > 10^{11}$ M$_\odot$) elliptical galaxies in the local Universe. Evidence tentatively suggests that these galaxies were assembled at high redshifts ($z \sim 3$–5), with the preceding starburst event taking place on short time-scales of $\sim$500 Myr (Thomas et al. 2010). One way to link galaxy populations formed at different redshifts is to derive their halo masses. Galaxy clustering provides a powerful method to constrain halo masses, particularly at high redshifts. Various clustering studies so far have revealed that passive galaxies cluster more strongly than their star-forming counterparts (Norberg et al. 2002; Ross & Brunner 2009; Williams et al. 2009; Hartley et al. 2010, 2013) and preferentially reside in more massive dark matter haloes. Hartley et al. (2013) analysed the clustering of passive galaxies by calculating two-point angular correlation functions for photometrically selected samples to $z \sim 3$, splitting their samples into bins of redshift and stellar mass. They found that passive galaxies are the most strongly clustered, residing in haloes of mass $M_{\rm halo} > 5 \times 10^{12}$ M$_\odot$. By establishing the typical host halo masses of high-redshift galaxies and the evolution of these halo masses to the present-day Universe, we can identify the possible progenitors of local massive elliptical galaxies.

A rare and interesting class of high-redshift galaxies is the population of ultra-luminous dusty galaxies with bright flux densities in the submillimetre waveband (Smail, Ivison & Blain 1997; Barger et al. 1998; Hughes et al. 1998). Known as submillimetre galaxies (SMGs), they appear to have redshift distributions peaking at $z \sim 2.5$ (e.g. Chapman et al. 2005; Simpson et al. 2014), occupying the same epoch associated with the peak activity of luminous AGN activity (Richards et al. 2006; Assef et al. 2011). The extreme luminosities observed in these dusty sources are thought to be powered by intense short-lived ($\sim$100 Myr) starbursts (Alexander et al. 2005; Tacconi et al. 2006, 2008; Ivison et al. 2011). Many previous studies (e.g. Hughes et al. 1998; Eales et al. 1999; Swinbank et al. 2006; Targett

et al. 2011) suggested that SMGs may be the progenitors of the most massive elliptical galaxies we see in the local Universe today. This scenario is tentatively supported by numerous clustering studies of SMGs identified in the long submillimetre wavelength bands (850–1100 μm; Webb et al. 2003; Blain et al. 2004; Weiß et al. 2009; Williams et al. 2011; Hickox et al. 2012), where observations of a strong clustering amplitude suggested SMGs resided in high-mass (10^{12}–10^{13} h^{-1}Mpc) dark matter haloes. Clustering studies of SMGs detected in the *Herschel* field (with shorter submillimetre wavelengths, 250–500 μm; e.g. Cooray et al. 2010; Maddox et al. 2010; Mitchell-Wynne et al. 2012; van Kampen et al. 2012) also confirmed strong SMG clustering signals. In fact, there may be evidence of an evolution of clustering with redshift, with Maddox et al. (2010) and van Kampen et al. (2012) reporting low clustering strengths for SMGs in redshifts $z < 0.3$. However, these studies may have been selecting different galaxy populations at low redshifts, compared to those identified at higher redshifts. In addition, many of these previous studies analysed only modest samples of SMGs (at most $\sim$100), and consequently halo masses were difficult to constrain.

Recently, however, we have obtained a much larger sample of SMGs. Technological advances with bolometer cameras, such as the SCUBA-2 camera on the 15 m James Clark Maxwell Telescope (JCMT), have allowed us to undertake submillimetre surveys over square degree areas down to mJy sensitivity limits (such as the SCUBA-2 Cosmology Legacy Survey or S2CLS; Holland et al. 2013; Geach et al. 2013). Chen et al. (2016a) used the radio and optical/infrared (IR) data from the Ultra-Deep Survey (UDS) to identify $\sim$1000 SMGs in the S2CLS field, making this the largest SMG sample so far in the 850 μm waveband. The increase of the sample size allowed Chen et al. (2016a) to make a clear detection in the two-point angular correlation function. However, the measurements still suffer from large uncertainties, and the evolution of SMG clustering is not constrained at all.

In this work, we make use of a cross-correlation technique to statistically associate the sample of SMGs to a much larger K-band-selected galaxy sample, which allows us to infer the dark matter halo mass with much greater confidence, and to constrain the evolution of SMG clustering for the first time. Fundamentally, by studying the dark matter haloes inhabited by these rare galaxies, we can identify their progenitors and descendants, helping us to understand the evolutionary link between extreme star-forming galaxies and those on the red sequence.

The structure of this paper is as follows. Section 2 contains the discussion of our data sets and sample selections; Section 3 describes our clustering analysis in greater detail; in Section 4, we show the results and discuss the implications; we end with our conclusions and further work in Sections 5 and 6. Throughout this paper we assume a Λ-CDM cosmology with $\Omega_{\rm M} = 0.3$, $\Omega_\Lambda = 0.7$, $H_0 = 70$ km s^{-1}Mpc^{-1} and $\sigma_8 = 0.9$. All magnitudes are given in the AB system, unless otherwise stated.

2 UDS DATA SET AND SAMPLE SELECTION

In this section, we introduce the SMG sample obtained from the S2CLS map of the United Kingdom Infrared Telescope (UKIRT) Deep Sky Survey (UKIDSS), UDS field, as well as passive and normal star-forming galaxies selected from the latter survey. We use K-band selected samples from the UKIDSS UDS Data Release 8, complemented by matching multiwavelength photometric data. Covering 0.77 deg^2, the UDS is a deep survey in the J, H and K wavebands. Reaching a depth of $K = 24.6$, it is the deepest near-IR

survey to date over such a large area. The final UDS data release (planned for mid-2016) will achieve estimated depths of $J = 25.4$, $H = 24.8$ and $K = 25.3$. The optical/IR catalogue used in this work is described in Hartley et al. (2013).

The UDS field is also covered by data in the B, V, R, i', z' optical bands from the Subaru *XMM–Newton* Deep Survey (Furusawa et al. 2008), the u-band from the Canada-France-Hawaii Telescope Megacam and three IR bands (two near-IR and one mid-IR) from the *Spitzer* UDS Legacy Program (SpUDS, PI:Dunlop). SpUDS provides data in channels 1 and 2 of InfraRed Array Camera (IRAC; 3.6 and 4.5 μm, respectively) as well as in the MIPS 24 μm waveband. After masking out bad regions and bright stars found in the UDS image, the co-incident area of these combined data sets is 0.62 deg². Finally, we use X-ray (Ueda et al. 2008) and radio (Simpson et al. 2006) observations to remove luminous AGN.

The SMGs were identified using the final 850 μm S2CLS maps of the UDS field (Chen et al. 2016a; Geach et al. 2016). Reaching a median depth of ∼0.9 mJy per beam, these maps are taken from the SCUBA-2 camera at the JCMT. The SCUBA-2 map in the UDS field has a noise of 0.82 mJy per beam at the deepest part, with rms noise <1.3 mJy over ∼1.0 deg². Compared to the LABOCA survey in the ECDF-S (LESS; Weiß et al. 2009), our map is ∼40 per cent deeper in sensitivity and has a ∼30 per cent improvement in spatial resolution, producing the largest sample of SMG identifications to date (6× larger than the LESS sample). We employ a robust sample of 716 SMGs detected at a significance of $>4\sigma$ from Chen et al. (2016a), in our clustering analysis.

2.1 Photometric redshifts and stellar masses

We use photometric redshifts in our analysis, obtained from the combination of deep photometry and a sample of over 3000 secure spectroscopic redshifts. Most redshifts at $z > 1$ were obtained from the UDSz ESO Large Programme (ID: 180.A-0776; PI: Almaini).

Using the EAZY template-fitting package (Brammer, van Dokkum & Coppi 2008), photometric redshift probability distributions were calculated for each object through a maximum likelihood analysis [see Hartley et al. (2013) and Mortlock et al. (2013) for further details]. The template fitting made use of the six standard EAZY templates and an additional template, a combination of the bluest EAZY template and a small amount of Small Magellanic Cloud-like extinction (Prevot et al. 1984). We train the fitting on the spectroscopic sample by comparing their spectroscopic redshifts to their derived photometric redshifts. Excluding outliers [$(z_{phot} - z_{spec})/(1 + z) > 0.15$, <4 per cent of objects], we find the dispersion in $(z_{phot} - z_{spec})/(1 + z)$ to be $\sigma = 0.031$. We have 242 passive and 1131 star-forming galaxies (separated using our *UVJ* selection, as discussed in Section 2.3) with spectroscopic redshifts, which are found to be in good agreement with their derived photometric redshifts. We find the dispersions in $(z_{phot} - z_{spec})/(1 + z)$ to be $\sigma = 0.023$ and $\sigma = 0.033$, respectively, with an outlier fraction of ∼3 per cent for both populations. However, we must note here that we have only 10 SMGs for which we have spectroscopic data, stressing the importance of using photometrically derived redshifts in this analysis. Investigating the robustness of photometric redshifts for this population is difficult due to the low number of sources. Nevertheless, we estimate a dispersion of $\sigma = 0.027$, with an outlier fraction of 10 per cent (one object), giving us confidence that photometric redshifts derived for SMGs are reasonable. Of the 10 SMGs with spectroscopic redshifts, only 5 reside at $z > 1$, the minimum redshift limit we consider for our analysis.

For our clustering analysis, we make use of the full probability distribution, similar to the approach adopted by Wake et al. (2011) and Hartley et al. (2013). A galaxy can have multiple entries across each redshift slice, whose contribution is weighted by the integrated probability between the limits of the redshift slices. We recompute stellar masses and rest-frame colours for each entry, at the minimum χ^2 redshift within the interval. We note that the redshift probability distributions typically become broader with increasing redshift, as also suggested from the overall comparison of spectroscopic and photometric redshifts, but this information is contained within the weighting system; pairs of galaxies with broad redshift distributions will make a smaller contribution to the clustering analysis. Further spectroscopic redshifts for SMGs will be required to determine if the probability distributions are accurate for this population. We note, however, that using the single best-fitting redshifts in our clustering analysis gives similar results, albeit with larger uncertainties.

Stellar masses were obtained from the same approach used by Hartley et al. (2013) and Mortlock et al. (2013, 2015). We fitted $u'BVRi'z'JHK$ bands and IRAC channels 1 and 2 to a grid of spectral energy distributions (SEDs). These SEDs were composed from Bruzual & Charlot (2003) stellar population models and a Chabrier initial mass function was assumed for the calculations. The star formation histories (with a variety of ages, dust extinctions and metallicities) were modelled by an exponentially declining star formation. The grid of synthetic SEDs was scaled to the K-band magnitude of the galaxy we wished to fit. Each scaled template was then fitted to the observed photometry, with stellar masses computed from the best-fitting template. We refer readers to the Hartley et al. (2013) and Mortlock et al. (2013) papers for a more in-depth discussion of the stellar mass derivation.

2.2 Sample selection – submillimetre galaxies

Chen et al. (2016a, hereafter C16) identified the counterpart candidates for the SCUBA-2 detected sources by using a combined radio and optical/IR colour method. This was trained on a sample of 52 SMGs in the UDS region, with identifications provided by the Atacama Large Millimeter/submillimeter Array (ALMA; Simpson et al. 2015a,b), as well as the ALMA-identified ALESS survey (Hodge et al. 2013). We briefly summarize the method here, referring readers to C16 for further details. C16 first identified any radio sources from a deep 1.46 Hz Very Large Array survey of the field that matched the SMGs to within 8.7 arcsec of the ALMA primary beam. Using the ALMA training sets in the UDS and ALESS, they showed that these radio-identified SMGs usually corresponded to the brightest component in a single-dish source. In addition, C16 also included the radio-undetected, K-selected sources that satisfied the Optical–Infrared Triple Colour (OIRTC) criteria. C16 used a new colour selection technique that is based on the fact that SMGs occupy a distinct parameter space in $z - K$, $K - m_{3.6}$ and $m_{3.6} - m_{4.5}$ colours, making it a useful method to separate SMGs from non-SMG field galaxies. This OIRTC selection is suitable for identifying the fainter counterparts to the SCUBA-2 sources, complementary to the radio detection of the brightest SMGs.

Consequently, we used the radio and OIRTC identifications from C16 to construct the sample of SMG counterparts used for this work. C16 adopted a search radius of 8.7 arcsec within the SCUBA-2 beam, in which this radius corresponds to a 4σ positional uncertainty for a 4σ SCUBA-2 detection. We note that the search radius is the same as the width of the ALMA primary beam used to derive the training sample. Based on the ALMA training sample, the combined radio+OIRTC selection method identified SMGs with an

accuracy of 83^{+17}_{-19} per cent and a completeness of 67 ± 14 per cent. Here we define the accuracy to be the fraction ($N_{\text{confirmed}}/N_{\text{selected}}$) of the selected candidate counterparts based on the selection methods (N_{selected}) that matched the selected candidates confirmed by ALMA ($N_{\text{confirmed}}$). For the parent sample of 716 $>4\sigma$ robustly detected submillimetre sources in the UDS, we consider only the sources that are covered by both radio and IR/optical data (Class 1, as defined in C16). Applying the radio + OIRTC selection technique on these 523 Class 1 sources, C16 found counterparts for 80 per cent of these (421/523), of which 37 ± 3 per cent have multiple counterparts. Sources for which C16 found no counterparts are not considered in this analysis. Adding all the Class 1 counterparts (including the multiple counterparts) together, the selection technique extracted a total of 610 SMG counterparts from 421 submillimetre sources, which we use for the rest of our analysis. We have repeated our clustering analysis using only one counterpart for each source (except for those that we have no counterparts for), finding consistent results within the uncertainties. While the clustering does change on small scales, we determine halo masses by fitting to the large-scale clustering only (see Section 3).

We apply additional quality cuts on the samples. A maximum limit on minimum χ^2 values obtained in photometric redshift fitting can be used to increase the reliability of source redshifts and to reduce contamination. A stellar mass completeness cut can also be applied to ensure that a proportion of galaxies with stellar masses above some limit would be detected. We present clustering measurements of SMGs with photometric redshift $\chi^2 < 20$ fits, which remove 8 per cent of the SMG sample. We do, however, note that SMG stellar masses are also uncertain, as the constraints on stellar masses from dusty SEDs are poor. We apply no mass cut on the SMGs; however, most of the SMGs appear to be massive with little dependence on redshift. Overall, $\sim$85 per cent of SMGs have stellar masses above the 90 per cent mass completeness limit (at $z = 3.5$) imposed on the passive and star-forming galaxies ($M_* > 10^{10.2}\,\mathrm{M_\odot}$, see Section 2.3). Repeating our clustering analysis after imposing this mass cut on SMGs yielded little difference in our clustering measurements, albeit with slightly larger uncertainties. Hence, we believe that making the mass cut is superfluous and we choose to keep all $\chi^2 < 20$ SMGs irrespective of their stellar mass for our analysis. We have also repeated our clustering measurements using various cuts in χ^2, K-band magnitude and redshifts. Adopting more conservative cuts, we found consistent results, while the size of the errors of our measurements increased due to reduced numbers in each redshift interval.

To test the redshift dependence of our clustering measurements, we split our sample by its redshifts. We present the redshift probability distribution of our samples in Fig. 1. To ensure a reasonable number of SMGs per redshift bin we use intervals of width $\Delta z = 0.5$, spanning the redshift range $1.0 < z < 3.5$ (see Table 1). We note that the number of SMGs given in Table 1 accounts for the fact that galaxies can be represented multiple times across different redshifts as previously described, each with a weight determined by its redshift probability distributions. The sums of these weights, representing the expected number of galaxies for a given redshift interval, are also listed in Table 1.

2.3 Sample selection – passive and star-forming galaxies

To enable us to place our clustering results in the context of galaxy evolution, we compare the SMG clustering to those of the star-forming and passive galaxies at the same redshifts. Taking the parent sample (after separating out the SMGs), we select the comparison
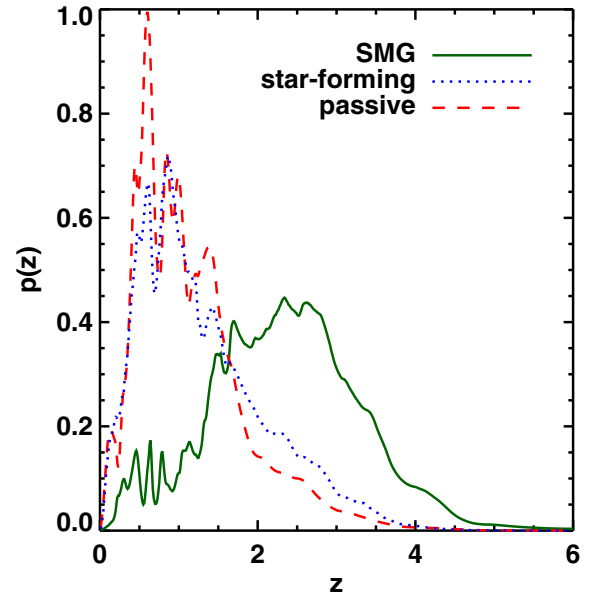

Figure 1. The redshift probability distributions for submillimetre, star-forming and passive galaxies. The SMGs are mostly located at redshifts $1.0 < z < 3.5$, influencing our choice of redshift intervals used in the cross-correlation analysis.

populations using the U, V and J-Bessel band rest-frame luminosities and subject them to colour criteria that are similar to those derived by Williams et al. (2009) and Hartley et al. (2013). In order to obtain cleaner samples of star-forming and passive galaxies, we refine our selection method by choosing quiescent galaxies that were classified by both the UVJ method and an independent PCA method (Wild et al. 2014). We shift the UVJ demarcation line from Hartley et al. (2013) to select passive galaxies as follows:

$$(U - V) > 0.88 \times (V - J) + 0.89 \quad (z < 0.5)$$

$$(U - V) > 0.88 \times (V - J) + 0.79 \quad (0.5 < z < 1.0)$$

$$(U - V) > 0.88 \times (V - J) + 0.69 \quad (z > 1.0)$$

with $U - V > 1.5$ and $V - J < 1.4$ at all redshifts. We repeated our clustering analysis using the original selection in Hartley et al. (2013), finding similar results, albeit with marginally less separation of passive and star-forming clustering amplitudes. While this criterion correctly identifies most of these galaxies, the passive sample is still likely to be contaminated by dusty star-forming galaxies that appear to be red and also galaxies hosting AGN. To identify dusty contaminants (those that have not already been identified as SMGs), we use 24 μm data and apply the methodology of Hartley et al. (2013). Passive galaxies with specific star formation rates $\mathrm{SSFR_{24\,\mu m}} > 7.43 \times 10^{-11}\,\mathrm{yr^{-1}}$, composing 3 per cent of UVJ-selected passive galaxies, are reassigned to the star-forming sample.

We sort our comparison samples into the same redshift intervals used for the SMG sample and imposed the same quality cuts to further clean our subsamples; galaxies with $\chi^2 > 20$ (from photometric redshift fits) were excluded to remove those that cannot be assigned a reliable redshift. Applying a K-band magnitude cut of $K = 24.3$ on our passive and star-forming samples, we impose a mass cut of $M_* > 10^{10.2}\,\mathrm{M_\odot}$, the 90 per cent mass completeness limit (up to $z = 3.5$). This cut ensures we are comparing passive and star-forming galaxies of the same stellar mass across all redshift intervals. We derive this limit using the methodology of Pozzetti et al.

Table 1. Table of clustering measurements used in Fig. 4. The columns shown are: number of galaxies, the sum of weights (the expected number of galaxies from the redshift probability distributions), redshift intervals, galaxy bias (plotted in Fig. 4), 1σ uncertainty on the bias, the clustering strengths (in units of h^{-1} Mpc) and their 1σ uncertainties, estimated blending bias (bb) for SMGs (see Section 4.3) and SMG galaxy bias corrected for blending bias.

N_{gal}	Σ_{weight}	z_{min}	z_{max}	b	σ_b	r_0	bb	b_{corr}
Sub-millimetre								
61	39.95	1.0	1.5	1.20	0.89	$3.19^{+2.72}_{-2.48}$	1.28	0.94
127	76.50	1.5	2.0	1.03	0.96	$2.19^{+2.36}_{-2.08}$	1.18	0.87
172	82.74	2.0	2.5	3.86	1.07	$7.98^{+2.48}_{-2.41}$	1.15	3.36
176	84.31	2.5	3.0	5.00	1.21	$9.08^{+2.47}_{-2.41}$	1.23	4.07
127	50.77	3.0	3.5	8.81	2.75	$14.87^{+5.24}_{-5.06}$	1.22	7.22
Radio sub-millimetre								
51	36.57	1.0	1.5	1.10	1.01	$2.89^{+3.07}_{-2.71}$	1.28	0.87
70	45.72	1.5	2.0	1.65	1.09	$3.69^{+2.79}_{-2.58}$	1.18	1.40
78	43.55	2.0	2.5	2.81	1.48	$5.59^{+3.15}_{-3.15}$	1.15	2.44
64	31.46	2.5	3.0	5.93	2.14	$10.98^{+4.48}_{-4.30}$	1.22	4.86
Star-forming								
706	540.61	0.0	0.5	0.53	0.15	$2.16^{+0.69}_{-0.67}$	–	–
2208	1774.09	0.5	1.0	0.88	0.13	$2.87^{+0.48}_{-0.47}$	–	–
2664	1854.41	1.0	1.5	1.92	0.14	$5.37^{+0.44}_{-0.43}$	–	–
2231	1351.12	1.5	2.0	1.81	0.21	$4.09^{+0.53}_{-0.52}$	–	–
1840	914.25	2.0	2.5	3.69	0.37	$7.56^{+0.85}_{-0.84}$	–	–
1275	639.00	2.5	3.0	5.25	0.52	$9.59^{+1.06}_{-1.05}$	–	–
Passive								
480	398.07	0.0	0.5	0.95	0.22	$4.13^{+1.07}_{-1.05}$	–	–
2160	1809.48	0.5	1.0	1.83	0.14	$6.48^{+0.55}_{-0.55}$	–	–
2219	1678.81	1.0	1.5	2.45	0.15	$7.04^{+0.48}_{-0.48}$	–	–
1423	936.83	1.5	2.0	2.60	0.25	$6.12^{+0.66}_{-0.65}$	–	–
739	350.28	2.0	2.5	6.24	0.59	$13.55^{+1.43}_{-1.42}$	–	–
531	228.49	2.5	3.0	7.69	0.74	$14.65^{+1.57}_{-1.56}$	–	–
Star-forming+Passive								
1018	457.22	3.0	3.5	5.01	1.09	$7.94^{+1.94}_{-1.89}$	–	–

(2010) and the implementation described in Hartley et al. (2013). We fit a second-order polynomial to the redshift-dependent mass limits ($M_{lim} = -0.13z^2 + 1.07z + 8.00$, in log solar mass units). For the volume-limited tracer galaxy population used in the cross-correlation analysis, we apply this redshift-dependent mass completeness limit and reject galaxies with stellar masses below M_{lim}. We caution that the *UVJ* selection becomes increasingly unreliable for $z > 3$, making passive galaxies difficult to identify correctly. Therefore, for the highest-redshift interval, we combine the passive and star-forming samples together into a combined sample of 1018 galaxies. We use these samples to compare the clustering of SMGs with those of typical star-forming and passive galaxies within the same redshift intervals. We give details of the various samples in Table 1.

3 CLUSTERING ANALYSIS

To analyse the clustering properties of galaxy populations, we evaluate the two-point autocorrelation function (ACF). Because we detect galaxies on a 2D-projected surface, we use the angular version of this function, a projection of the three-dimensional spatial correlation function (Peebles 1980). The ACF provides us a robust way of tracing the dependence of large-scale structure on galaxy properties and evolution through redshift.

The ACF, $w(\theta)$, is a measure of the excess probability, compared with a random distribution, of finding a galaxy at an angular separation θ from another galaxy. We use the Landy & Szalay (1993) estimator, described by

$$w(\theta) = \frac{DD(\theta) - 2DR(\theta) + RR(\theta)}{RR(\theta)}, \tag{1}$$

where $DD(\theta)$, $DR(\theta)$ and $RR(\theta)$ are the galaxy–galaxy, galaxy–random and random–random normalized pair counts, respectively.

We note that our observed field is finite in size, which can lead to an underestimation of the clustering by a factor that is defined as the integral constraint. We use the formalism of Roche & Eales (1999),

$$C = \frac{\sum RR(\theta).w(\theta)}{\sum RR(\theta)}, \tag{2}$$

which is dependent on the intrinsic clustering of galaxies, normally by adopting some form for $w(\theta)$. Following the method of Hartley

et al. ([2013](#)), we assume $w(\theta)$ to be the angular correlation function of the underlying dark matter distribution traced by galaxy populations.

To obtain the dark matter correlation function, we determine the nonlinear power spectrum, using the formalism of Smith et al. ([2003](#)). Using the redshift probability distribution, $p(z)$, of the galaxy population, we Fourier transform the spectrum and project it to calculate the dark matter correlation function. We then compute the galaxy bias, a measure of how well galaxies trace the dark matter distribution. This is quantified by the following relationship:

$$w_{\mathrm{obs}}(\theta) = b^2 \times w_{\mathrm{dm}}(\theta), \tag{3}$$

where w_{obs} and w_{dm} are the correlation functions of the observed galaxy population and dark matter distribution, respectively. The fitting of the dark matter correlation function to the observed galaxy correlation function is done by minimizing the χ^2. Galaxies having a large bias are more likely to be found near the highest density peaks in the dark matter mass distribution.

The galaxy bias is dependent on the dark matter halo mass and the galaxy formation epoch, as described by Mo & White ([1996](#)). At large scales, w_{dm} and w_{obs} are consistent in both the linear (w_{linear}) and nonlinear ($w_{\mathrm{nonlinear}}$) correlation regimes, where the ACFs are well described by linear gravity theory. At small scales however, they deviate; nonlinear effects become more significant and we can no longer assume that the galaxy population traces the dark matter distribution. We adopt the transition limit between the linear and nonlinear scales, $w_{\mathrm{nonlinear}} < 3 \times w_{\mathrm{linear}}$, in order to constrain the fitting of both the integral constraint and the bias at large scales. We also apply an upper limit of $\theta = 0°.4$ of separation to this fit, beyond which our measurements become unreliable due to the reduced area resulting from our finite field of view.

Attempting to derive the ACF on small data sets is likely to produce large statistical errors, reducing our ability to derive well-constrained halo masses. Since we have a small sample of submillimetre galaxies at $1.0 < z < 3.5$, the ACF is not sufficient for a reliable clustering analysis on our sample (see C16).

However, we can apply a closely related correlation function: the two-point cross-correlation function (CCF), using the positions of the much larger sample of K-band-selected galaxies. We cross-correlate the desired sample population (D_{s}) with a full volume-limited 90 per cent mass-complete tracer population (D_{t}), as follows:

$$w(\theta) = \frac{D_{\mathrm{s}}D_{\mathrm{t}}(\theta) - D_{\mathrm{s}}R(\theta) - D_{\mathrm{t}}R(\theta) + RR(\theta)}{RR(\theta)}, \tag{4}$$

where both data sets are normalized by the total pair counts. By cross-correlating a small target sample (SMGs) with a large tracer population (normal K-selected galaxies), the cross-correlation function greatly increases the number of pairs, achieving greatly reduced statistical uncertainties, compared to the autocorrelation. Because each galaxy's contribution to a redshift slice is weighted by its probability distribution between the given redshift interval limits (see Section 2.1), we must apply a weighting scheme to the pair counts. Instead of using a simple pair count, the pair counts we calculate are the sum of the products of these weights over pairs of objects. Evaluating the ACF of the large tracer population and the CCF of the target sample crossed with the tracer, we inferred the bias of the tracer population (b_{t}) and the CCF bias, b_{st} [using equation (3)]. Finally, the bias of the sample population, b_{s}, is calculated:

$$b_{\mathrm{s}} = \frac{b_{\mathrm{st}}^2}{b_{\mathrm{t}}}. \tag{5}$$

We infer the ACF of the target sample population by multiplying out the tracer population bias from the ccf by ($b_{\mathrm{ccf}}^2/b_{\mathrm{tracer}}^2$), allowing us to compare the ACF of all sample populations. We ensure that the sample size of the random points is at least $10\times$ larger than that of the tracer population. The errors derived from the ACF and CCF are estimated using a bootstrap analysis with 100 repetitions, by resampling the galaxy population with replacement. We calculate $w(\theta)$ for each of the 100 bootstrap samples and derive the variance on $w(\theta)$. We have made the assumption that both the sample and the tracer populations trace the same dark matter distribution and that both are linearly biased.

Finally, we estimate the halo masses of our samples using the Mo & White ([2002](#)) formalism. We also estimate the correlation length, r_0, using the formalism of Peebles ([1980](#)). This quantity is related to the bias parameter as follows:

$$r_0 = 8 \left(\frac{\Delta_8^2}{C_\gamma} \right)^{\frac{1}{\gamma}}, \tag{6}$$

where Δ_8 is the clustering strength of haloes, more massive than the stellar mass M at redshift z, defined as $\Delta_8 = b(M, z)\sigma_8 D(z)$. The function $D(z)$, as defined by $D(z) = g(z)/[g(0)(1 + z)]$, measures the growth factor of linear fluctuations in the dark matter distribution [see, for example Mo & White ([2002](#))], with

$$g(z) = \frac{5}{2}\Omega_{\mathrm{m}}[\Omega_{\mathrm{m}}^{4/7} - \Omega_\Lambda + (1 + \Omega_{\mathrm{m}}/2)(1 + \Omega_\Lambda/70)]^{-1}. \tag{7}$$

To maintain a reliable clustering estimate and ensure robust conclusions, we impose a lower limit of sample sizes required for the analysis; if a subsample for a given redshift interval contains fewer than 30 objects, we do not include it in the analysis presented here.

4 RESULTS AND DISCUSSION

4.1 Clustering of $1 < z < 3$ SMGs and comparison to previous literature

Previous studies of SMG clustering have focused on the broad redshift range $1 < z < 3$ (Webb et al. [2003](#); Blain et al. [2004](#); Weiß et al. [2009](#); Williams et al. [2011](#); Hickox et al. [2012](#)). The majority of SMGs in our sample also lie in this key redshift range, as shown in Fig. [1](#). To directly compare with previous clustering measurements, we first apply our clustering methodology (as described in Section 3) on the 365 SMGs ($\Sigma_{\mathrm{weight}} = 284$) located in the redshift range $1 < z < 3$. Cross-correlating all the SMGs in the redshift range $1 < z < 3$ with a 90 per cent mass-complete tracer sample (normal K-selected galaxies) yielded the galaxy bias value $b = 2.18 \pm 0.97$ and correlation length $r_0 = 4.1^{+2.1}_{-2.0}\ h^{-1}$ Mpc. Using the formalism of Mo & White ([2002](#)), our result corresponds to a halo mass of $M_{\mathrm{halo}} \sim 10^{12}\ \mathrm{M}_\odot$. We plot this in Fig. [2](#), with the accompanying correlation functions, comparing with various previous measurements.

From Fig. [2](#), we find that our clustering measurement is low, but consistent within the errors, when compared to the previous results. In particular, our result shows good agreement with that of Blain et al. ([2004](#)) [corrected by Adelberger et al. ([2005](#))] and Hickox et al. ([2012](#)). The consistency with Blain et al. ([2004](#)) improves further if we compare with their reported alternative clustering strength ($r_0 = 5.5 \pm 1.8\ h^{-1}$ Mpc) in the absence of the SSA22 field, the most overdense field surveyed in their investigation and a well-known proto-cluster region (Steidel et al. [1998](#)). We note that our sample is $\sim 5\times$ larger than that of Hickox et al. ([2012](#)), which used
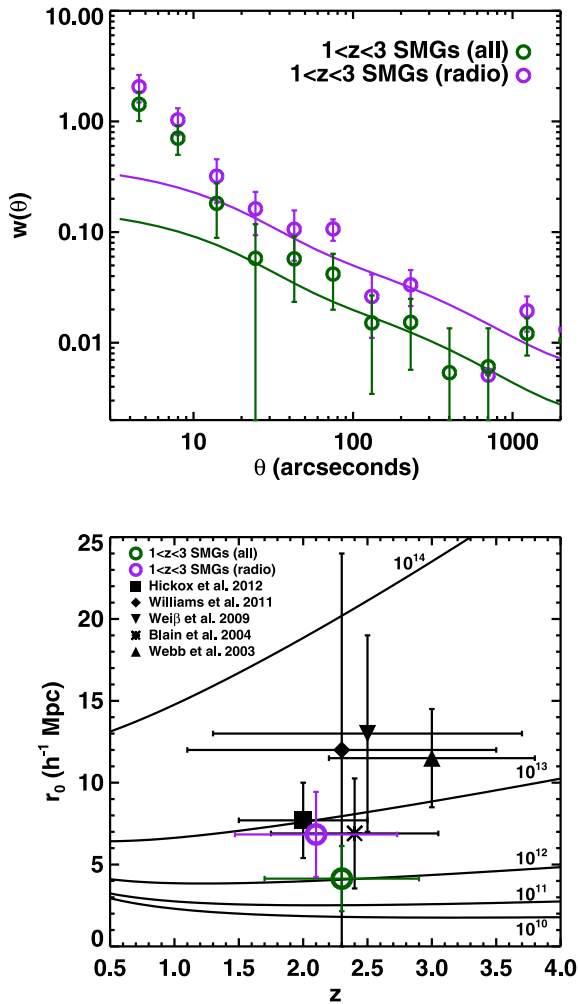
Figure 2. Top panel: the correlation functions for all $1 < z < 3$ submillimetre galaxies and the subset of radio-detected submillimetre galaxies. The correlation functions are determined by multiplying their corresponding cross-correlation functions by (b_{CCF}^2/b_{tracer}^2), where b is the galaxy bias. The solid lines are dark matter correlation functions fitted on to the observed galaxy correlation functions. Bottom panel: the clustering strength r_0 as a function of redshift. Open green and purple points are clustering measurements of all the SMGs and SMGs identified with the radio counterparts, respectively, at redshifts $1 < z < 3$. The black points are clustering results from previous studies: Webb et al. (2003), Blain et al. (2004), Weiß et al. (2009), Williams et al. (2011) and Hickox et al. (2012). The curves represent the predicted clustering strengths for dark matter haloes of varying masses (labelled, in solar masses), produced using the formalism of Mo & White (2002).

the largest SMG sample in a similar analysis prior to this study. Our measured clustering strengths are also consistent with previous clustering studies of IR galaxies selected at shorter wavelengths (e.g. Farrah et al. 2006; Cooray et al. 2010; Maddox et al. 2010; Mitchell-Wynne et al. 2012, where the latter three studied SMGs in the *Herschel* field).

It appears at first sight that, on average, SMGs are not as strongly clustered as previously thought. Alternatively, the SMG clustering could be more complex and may be dependent on redshift, large-scale environment and merger history. Chapman et al. (2009) discussed the dependence of a complex bias on the large-scale environment and merger history. They proposed that SMGs may reside

in smaller haloes than would be inferred from the linear bias model assumed in the halo modelling for this study. In that case, SMGs do not necessarily trace the most massive dark matter haloes in the Universe.

The relatively low clustering measurement we derive may be affected by the complex nature of SMG clustering that evolves with redshift. Limiting our redshift interval size to $1.5 < z < 3.0$ and cross-correlating the resulting sample of 327 SMGs ($\Sigma_{weight} = 244$), we find SMGs are more strongly clustered, with a bias $b = 4.40 \pm 0.86$, in better agreement with previous studies. This stronger clustering signal suggests that the excluded low-redshift SMGs are weakly clustered and they are diluting the stronger clustering exhibited by higher-redshift SMGs. This indicates a possible redshift evolution in SMG clustering, which we explore, in detail, in Section 4.2.

Previous studies had small sample sizes, typically comprising the more luminous (radio-identified) SMGs. In contrast, our sample of SMGs includes many fainter counterparts and a significant fraction ($\sim$50 per cent) having no strong radio emission. Therefore, it is possible that previous clustering measurements were biased towards the brightest radio SMGs, which may be a more extreme luminous subset of the SMG population. To test this claim, in Fig. 2, we present the clustering measurement of SMGs that have radio counterparts only. We find radio SMGs to be slightly more strongly clustered with respect to all SMGs, with bias $b = 3.20 \pm 1.12$, correlation length $r_0 = 6.8^{+2.7}_{-2.6}$ h^{-1} Mpc and halo mass $M_{halo} \sim 10^{13}$ M$_\odot$. This measurement is also consistent with previous studies, in good agreement with Blain et al. (2004) and Hickox et al. (2012), within 1σ errors. The improved consistency suggests that the previously studied higher luminosity radio SMGs tend to reside in higher mass haloes. Investigating the possibility of the clustering dependence on radio emission and $S_{850\,\mu m}$ flux density further would require a much larger sample of SMGs than even we have presently. We attempted to measure the clustering strength as a function of $S_{850\,\mu m}$ flux density for the SMG sample at redshifts $1 < z < 3$. We found no significant trend, however, since the uncertainties were too large.

Finally, it is worth noting that clustering measurements performed with single-dish surveys are subjected to a blending bias (e.g. Hodge et al. 2013; Karim et al. 2013; Cowley et al. 2016). This describes the contribution to the clustering signal due to the blending of SMGs into single submillimetre sources as a result of the low resolution. We discuss this in detail in Section 4.3. Summarizing briefly, Cowley et al. (2016) simulated this effect at 850 µm to match observations in the SCUBA-2 map. They suggest that the confusion between the sources can artificially increase the galaxy bias measurements by a factor of $\sim$2 and that any galaxy bias measured with a single-dish survey must be corrected for by this factor. We note that the factor $\sim$4 derived in Cowley et al. (2016) applies to the clustering amplitude, A, for which this quantity scales with the galaxy bias squared b^2. In addition, surveys with larger beams are subjected to a greater blending bias. The Hickox et al. (2012) and Weiß et al. (2009) clustering measurements were carried out with the ECDFS LABOCA survey, which has a full width at half-maximum beam of $\sim$20 arcsec. Similarly, Williams et al. (2011) utilized the 28 arcsec Astronomical Thermal Emission Camera (AzTEC; on the Atacama Submillimeter Telescope Experiment) beam, selecting SMGs at 1100 µm. The clustering measurements in the previous literature could therefore be subjected to a larger correction than the value derived for the current SCUBA-2 survey. It is likely that correcting for blending would bring previous studies into better agreement with the clustering measurements presented here.

4.2 Evolution of SMG halo masses with redshift

Having a large sample of SMGs in a single field, we can now test the redshift dependence of SMG clustering derived using a cross-correlation technique. We also compare the clustering measurements with those of the *UVJ*-selected passive and star-forming galaxies to reveal their possible relation to SMGs. Splitting the sample into the redshift intervals described in Section 2.2 and applying the cross-correlation analysis in Section 3, we plot the resulting correlation functions in Fig. 3. We compare the clustering of SMGs, passive and star-forming galaxies in each of the redshift intervals. As noted earlier, in the highest-redshift interval ($3.0 < z < 3.5$), we combine the passive and star-forming objects into a single sample containing both populations as we can no longer rely on the *UVJ* selection at such high redshifts. For clarity, we plot error bars for the SMG correlation functions only. The ACFs are derived from their respective cross-correlation functions multiplied by (b_{CCF}^2/b_{tracer}^2).

From the 2D (projected on sky) representation of clustering, we find that passive galaxies exhibit stronger clustering amplitudes with respect to their star-forming counterparts, at all redshifts up to $z = 3$. This is in good agreement with previous studies, including Hartley et al. (2013), who also studied the UDS field. SMGs, however, appear to have a range of clustering amplitudes in different redshift intervals. At $1 < z < 2$, SMGs appear to be weakly clustered, consistent with their normal star-forming counterparts. At $z > 2$, the SMG correlation functions are consistent with those of both the passive and star-forming samples, within 1σ. The results for the redshift range $3.0 < z < 3.5$ suggest that the highest-redshift SMGs are tentatively more clustered than normal galaxies, on average.

For a more intuitive representation of the clustering results, in Fig. 4 we plot the bias measurements computed from the cross-correlation methodology in Section 3 and relate them to halo masses using the Mo & White (2002) formalism. We also list the bias measurements and their uncertainties in Table 1. From Fig. 4, a number of trends are apparent. First, we find that passive galaxies reside in dark matter haloes of mass $\sim 10^{13}$ M$_\odot$, consistent across most redshift intervals [in good agreement with Hartley et al. (2013)]. On the other hand, star-forming galaxies are clearly more weakly clustered than their passive counterparts, residing in low-mass haloes ($\sim 10^{10}$–10^{12} M$_\odot$) up to redshift $z \sim 2$. At higher redshifts, the star-forming galaxies appear to reside in haloes of increasingly higher mass. Thus, star-forming galaxies show evidence for downsizing, with activity shifting towards lower-mass haloes as the Universe ages. Our expectations of the relative clustering between passive and star-forming objects are confirmed, with our results reflecting the findings of numerous previous studies (e.g. Meneux et al. 2006; Williams et al. 2009; Furusawa et al. 2011; Wake et al. 2011; Jullo et al. 2012; Hartley et al. 2013).

To place these clustering results in context, we discuss a common feature in many galaxy evolution models, the hot-halo scenario, which suggests that galaxy evolution is dependent on dark matter halo mass (e.g. Croton et al. 2006; Cen 2011; McCracken et al. 2015; Lin et al. 2016). A dark matter halo growing in mass becomes more effective in maintaining a reservoir of gas with cooling times longer than the age of the Universe (e.g. a few Gyrs). Any additional gas infalling into the halo is shock heated and is prevented from forming stars. The virial temperature of the dark matter halo will continue to increase from the accretion of more haloes while reservoirs of cold gas within any galaxy in the halo become exhausted and SFRs in galaxies decline as they can no longer accrete. Galaxies that reside in more massive haloes will have their star formation increasingly quenched. This suggests that there is some threshold halo mass limit
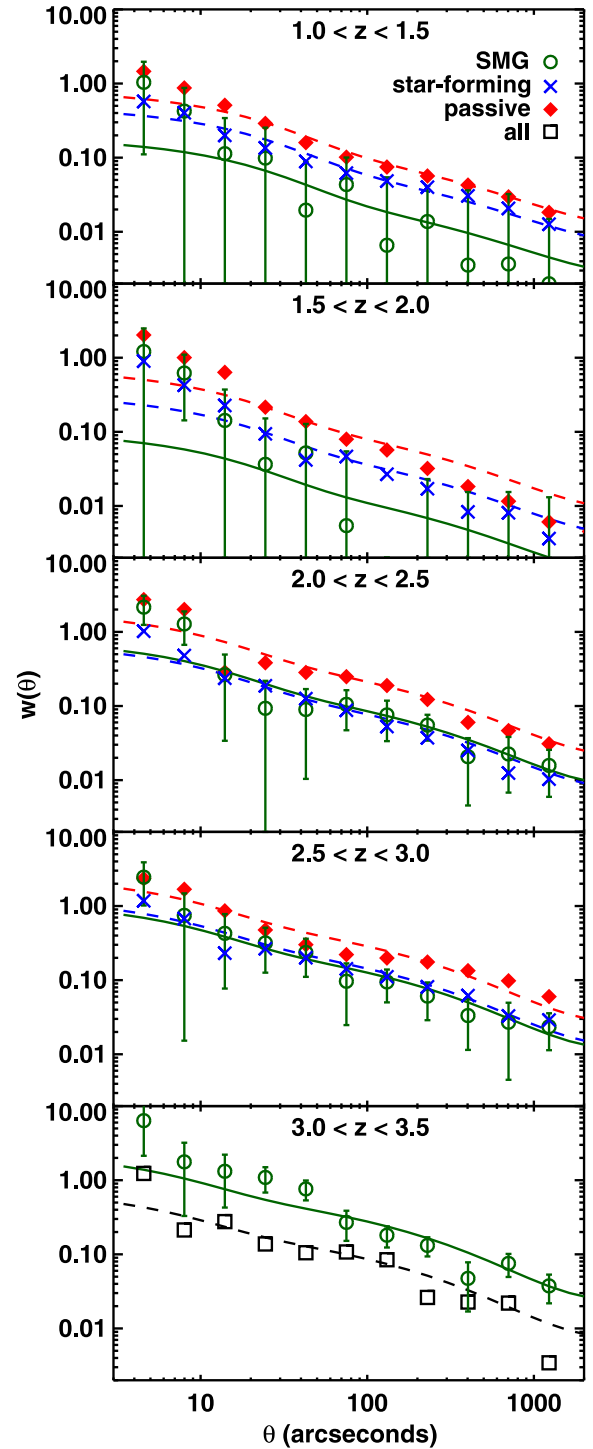

Figure 3. The correlation functions for submillimetre galaxies, compared with comparison samples of passive and star-forming *K*-band-selected galaxies. The correlation functions are determined by multiplying their corresponding cross-correlation functions by (b_{CCF}^2/b_{tracer}^2), where *b* is the galaxy bias. The panels represent redshift intervals as marked. The solid (dashed) lines are dark matter correlation functions fitted on to the observed SMG (passive and star-forming) correlation functions. For $3.0 < z < 3.5$, the black squares represent all detected galaxies minus SMGs. The error bars (typically of order $\sim$0.01) for the non-SMG samples have been omitted for clarity.
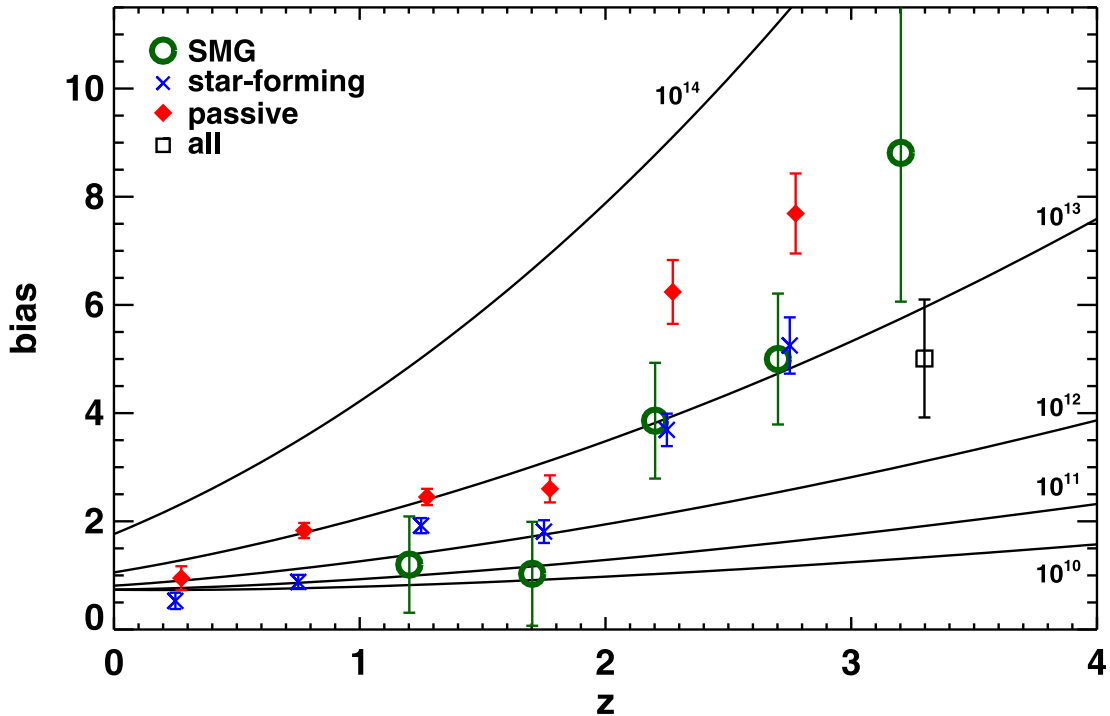
Figure 4. Galaxy bias versus redshift for submillimetre galaxies (open green circles), compared with a sample of *K*-band passive and star-forming galaxies (filled red diamonds and blue crosses, respectively). The points are offset slightly for clarity. The solid lines show the evolution of bias for dark matter haloes [produced using the formalism of Mo & White (2002)], with varying mass (labelled, in solar masses).

above which galaxies become progressively passive. According to recent models, this limit is of order of a few $\sim 10^{12}$ M$_\odot$ with maximum quenching at 10^{13} M$_\odot$ (Croton et al. 2006; Cen 2011), consistent with the derived halo masses for passive galaxies in this study.

Our population of interest, the SMGs, appears to exhibit a clustering signal that is dependent on redshift; the downsizing effect appears to be even stronger than seen in star-forming galaxies. The downsizing effect appears to confirm predictions made with the Hayward et al. (2013) mock SMG catalogues used by Miller et al. (2015). At $1 < z < 2$, SMGs reside in haloes of relatively low masses, $\sim 10^{11}$ M$_\odot$. This is consistent with star-forming galaxies, thus SMGs are weakly clustered at this epoch with respect to passive galaxies. As we advance to higher redshifts ($z > 2$), we see a stronger SMG clustering amplitude, although still consistent with star-forming galaxies. We compute halo masses $M_{halo} \sim 5.89 \times 10^{12}$ M$_\odot$ and $M_{halo} \sim 1.26 \times 10^{13}$ M$_\odot$ for redshift intervals $2.0 < z < 2.5$ and $2.5 < z < 3.0$, respectively. The results for these redshifts are in reasonable agreement with previous studies (Webb et al. 2003; Blain et al. 2004; Weiß et al. 2009; Williams et al. 2011; Hickox et al. 2012), and in contrast to the low SMG clustering amplitude at lower redshifts.

Comparing to galaxy populations selected at shorter wavelengths than the 850 µm sample used in this study, we find our estimated clustering measurements broadly consistent with a number of studies (e.g. Farrah et al. 2006; Cooray et al. 2010; Maddox et al. 2010; Mitchell-Wynne et al. 2012). Farrah et al. (2006) studied the spatial clustering of galaxies selected in the IRAC bands using a 1.6 µm emission feature, with SFRs similar to SMGs. Splitting the sample into two redshift bins between 1.5 and 3.0, the authors derived halo masses of $M_{halo} \sim 6 \times 10^{13}$ M$_\odot$, consistent with our measurements at the high-redshift bins. However, they reported no strong redshift evolution in the clustering of their selected galaxy samples. In con-

trast, Magliocchetti et al. (2013) found the same halo downsizing trend as reported in this study, having performed a clustering analysis on galaxies selected at wavelength 60 µm (SFR ≥ 100 M$_\odot$ yr^{-1}) in the Cosmological Evolution Survey (COSMOS; Scoville et al. 2007) and Extended Groth Strip fields.

The relatively weak SMG clustering seen at redshifts $1 < z < 2$ demonstrates that the SMGs at this epoch are unlikely to be the progenitors of the massive (~ 2–4 L*) elliptical galaxies we see in the local Universe. The typical bias measurements, halo masses and hence the environment of these elliptical galaxies do not match the measurements of the SMGs at redshifts $1 < z < 2$. This finding is emphasized in Fig. 5, where we plot the expected evolution of the dark matter bias for haloes with observed M_{halo} for SMGs. This evolution is calculated using the Fakhouri, Ma & Boylan-Kolchin (2010) formalism of the median growth rate of haloes, as a function of halo mass M_{halo} and redshift.

Tracing the growth of haloes over redshifts $1 < z < 2$, it is clear that haloes hosting SMGs at these redshifts do not evolve to become haloes hosting massive passive galaxies at the present day. This further supports the idea that these SMGs are not the progenitors of the massive elliptical galaxies we see today, which typically reside in haloes with a minimum mass of $\sim 10^{13}$ M$_\odot$ (e.g. Magliocchetti & Porciani 2003; Zehavi et al. 2011). However, haloes hosting SMGs in the redshift range $2.0 < z < 2.5$ are consistent with their low-redshift passive counterparts, emphasizing that in order for the SMGs to be these progenitors, they must typically form at redshifts $z > 2$. It is worth noting that in the highest-redshift intervals, $z > 2.5$, SMG host haloes would eventually evolve into very massive haloes ($M_{halo} > 10^{14}$ M$_\odot$), which typically host galaxy clusters at the present day (Estrada et al. 2009).

We place these findings further into their observational context by commenting on the following two previous studies of SMGs in
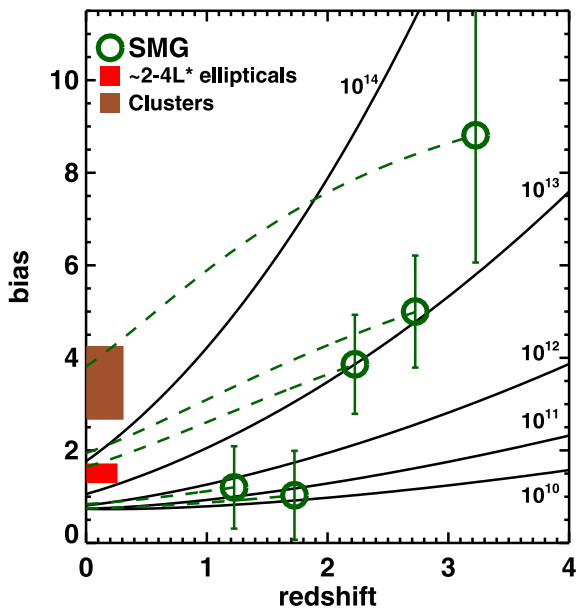
Figure 5. Predicted galaxy bias evolution of SMGs (open green circles) at $z > 1$, plotted against redshift. The solid black lines represent the expected bias evolution for dark matter haloes with constant masses (labelled, in solar masses). We trace the mass growth of haloes hosting SMGs in green dashed lines, using the formalism from Fakhouri et al. (2010). We also plot typical bias measurements of $\sim 2 - 4\,L^*$ galaxies [from the luminosity-bias relation derived in Zehavi et al. (2011)] and optically selected galaxy clusters at redshifts $0.1 < z < 0.3$ (Estrada, Sefusatti & Frieman 2009).

single clusters at different redshift epochs. First, Smail et al. (2014) studied a $z = 1.62$ cluster in the UKIDSS S2CLS, hosting a mix of massive passive galaxies and highly active galaxies with significant dust content. In summary, they found that the most active cluster members reside in the underdense regions in the cluster, while the dense cores are populated in this structure at this epoch by massive passive galaxies. Hence, massive galaxies in the dense cores of the local Universe were already likely to be in place at $z = 1.6$, and any ultraluminous star-forming galaxies found in this cluster of interest are likely to be infalling on to this structure. Therefore, the progenitors of these elliptical galaxies are likely to have undergone a transformation at $z > 2$.

The halo-downsizing phenomenon is further supported when we consider a second study, by Umehata et al. (2015), of a protocluster traced by Lyman α emitters (LAEs) at $z = 3.1$. Using the AzTEC, they detected 10 SMGs within this protocluster located in the SSA22 field. A cross-correlation technique with LAEs revealed that SMGs are strongly clustered and reside at the core of this protocluster. Additionally, Dannerbauer et al. (2014) found an excess of 870 µm selected SMGs in a protocluster associated with the radio galaxy MRC1138–262 at $z = 2.16$. If other protoclusters at this epoch host SMGs in their cores, then this finding would be consistent with the strong clustering amplitudes we measured for $z > 2$. Combining results from both Smail et al. (2014) and Umehata et al. (2015), it appears that SMG activity shifts from high-density environments at high redshifts to low-density environments at later epochs, as seen in our clustering results.

When considering the link of SMGs to the progenitors of local elliptical galaxies, we must make the following caveat; we also find normal star-forming galaxies in the same mass haloes as the SMGs, at every redshift interval. Because star-forming galaxies ex-

hibit clustering signals indistinguishable from SMGs, we cannot rule out the possibility that these normal galaxies at $z > 2$ could also evolve to become the local massive elliptical galaxies. Adopting this view, SMGs are just the more dusty highly star-forming subset of normal star-forming galaxies, found at the top of the main sequence. SFRs derived using far IR photometry (Michałowski et al. in preparation) reveal that most SMGs do indeed lie on the main sequence of star-forming galaxies, with an average SFR evolving with time, from $SFR_{av} \sim 360\,M_\odot\,yr^{-1}$ at redshifts $3.0 < z < 3.5$ to $SFR_{av} \sim 190\,M_\odot\,yr^{-1}$ at redshifts $1.0 < z < 1.5$. In contrast, measuring SFRs from optical/IR photometry of massive star-forming galaxies, we find a mean SFR of $\sim 100\,M_\odot\,yr^{-1}$, which has no significant evolution with redshift. It is therefore possible that optical/IR determinations are missing the most dust-enshrouded star formation, but we defer a detailed investigation of the relationship between SFR and halo mass to future work. For this work, we simply note the striking similarity between the clustering of SMGs and normal star-forming galaxies, suggesting no strong link between SFR and environment when comparing star-forming galaxies at a given epoch.

An alternative way to compare high-redshift star-forming galaxies with their possible descendants is to consider space densities. The number density of normal star-forming galaxies is found to be at least $\sim 2 \times 10^{-4}\,Mpc^{-3}$, which rises with decreasing redshift (up to $z = 1$). Considering that this is larger than the typical number density of local luminous red galaxies ($\simeq 10^{-4}\,Mpc^{-3}$, e.g. Wake et al. 2006), it is likely that most star-forming galaxies do not evolve to become these massive red systems by the present day. SMGs have low number densities of $\simeq 1$–$2 \times 10^{-5}\,Mpc^{-3}$, which remain constant across all redshift intervals considered in this study. By calculating the SMG number densities, we can estimate the number densities of the SMG descendants. Assuming that each SMG galaxy goes through one SMG phase in its lifetime, we determine the descendant number density, ϕ, using the simple relation,

$$\phi = \rho_{SMG} \times \frac{\tau_{obs}}{\tau_{burst}}, \qquad (8)$$

where ρ_{SMG} is the observed SMG number density, τ_{obs} is the time between each redshift interval considered and τ_{burst} is the SMG lifetime. We note that most of the uncertainty lies with the estimation of the SMG lifetime. Numerous previous studies estimated the lifetime to be $\sim 100\,Myr$, by using gas mass measurements from CO observations in SMGs (Chapman et al. 2005), estimating gas consumption time-scales and fading times (Swinbank et al. 2006) or employing simple stellar evolution models based on star formation time-scale (Hainline et al. 2011). Adopting $\tau_{burst} = 100\,Myr$ implies that the expected number densities will be $\phi \simeq 4 \times 10^{-5}$–$2 \times 10^{-4}\,Mpc^{-3}$, for SMGs at redshifts $1.0 < z < 3.5$. Interestingly, SMG descendants located at redshifts $2.0 < z < 2.5$ and $2.5 < z < 3.0$ are expected to have number densities of $\phi \simeq 1 \times 10^{-4}\,Mpc^{-3}$, in excellent agreement with the number density of luminous red galaxies. These arguments provide further evidence that SMGs located at redshifts $z \simeq 2$ are likely progenitors of these massive elliptical galaxies, while possibly eliminating the normal star-forming galaxies as candidates, on account of their higher number densities.

4.3 Uncertainties

We discuss here a number of uncertainties in our analysis. The construction of our sample could be performed in a variety of ways and although we believe that we have used the optimal selection method, there is no single correct method. The choice of cuts we

make with such a small sample of SMGs could significantly impact our clustering measurements. We have applied a variety of cuts on the χ^2 of the photometric redshift fitting and mass, as well as a selection of different redshift binning methods. It is, in essence, a compromise between securing large numbers of SMGs and maintaining high-quality photometric data. Varying the selection makes little qualitative difference to the conclusions of this work – in most cases, we see evidence of a downsizing effect on haloes hosting SMGs. However, our measurement in the lowest SMG redshift interval ($1.0 < z < 1.5$) is sensitive to the choice of selection. This variation is most likely due to the low number of SMGs in this bin (~60). While the clustering amplitudes in the higher redshift bins are relatively stable, in this bin we find variations in the bias measurement by up to a factor of 2, although formally always consistent with the star-forming galaxies at this epoch (Fig. 4). We conclude that larger samples are required for more robust measurements of clustering in this redshift range.

The low clustering measurements for redshifts $1 < z < 2$ may be attributed to the reliability of the SMG identifications. Because a lower clustering measurement corresponds to an increasingly random distribution of objects, this could reflect an increasing contamination in our low-redshift SMG sample. To test this scenario, we performed a clustering analysis on the SMGs with secure radio counterparts, whose selection technique is well established in previous literature (e.g. Ivison et al. 2002, 2005; Pope et al. 2006; Yun et al. 2012). The resulting bias and halo mass measurements, which we present in Table 1, are broadly consistent with those of the radio + OIR SMGs, especially at low redshifts ($1 < z < 2$). This is no surprise, however, as nearly all SMGs at lower redshifts are identified as radio counterparts (see Fig. 1), reflecting the fact that the radio selection technique is best at picking out the luminous SMGs at low redshifts. This complements the OIRTC selection, which is better at identifying less luminous SMGs at redshifts $z > 2$. Generally, SMGs selected using radio counterparts are skewed towards lower redshifts; the fraction of SMGs with radio counterparts reduce from 84 per cent at redshifts $1.0 < z < 1.5$ to 36 per cent at redshifts $2.5 < z < 3.0$. In fact, based on the ALMA training sample, the OIRTC and radio selection techniques both have the same completeness and accuracy, 52 ± 12 per cent and 87^{+13}_{-23} per cent, respectively (C16). We also note that the stellar mass distribution of radio SMGs is consistent with that of SMGs with combined OIRTC/radio counterparts (i.e. most of these galaxies have stellar masses $M_* > 10^{10.2}$ M$_\odot$), with no significant evolution with redshift. Hence, we are confident that the low-redshift SMGs are not heavily contaminated by misidentified galaxies and that the low-clustering amplitudes appear to reflect the scenario in which low-redshift SMGs live in lower-density environments compared to their high-redshift counterparts.

We also note that our SMG identification is incomplete, having associated counterparts with 80 per cent of the submillimetre sources. Hence, there are submillimetre sources whose clustering properties are not being measured. We remark that most of these sources tend to be fainter, in which the incompleteness fraction increases to ~30 per cent for sources with flux density $S_{850\,\mu m} <$ 5 mJy. These may be faint sources blending together to produce brighter submillimetre signals above the flux limit of 2.7 mJy, but for which no counterparts can be detected. Alternatively, they may be sources located at high redshifts ($z > 3$), for which the radio+OIR selection techniques are limited in their ability to identify SMGs. We attempt to measure the effect of the counterpart incompleteness on the clustering signal by calculating the ACF of all 4σ sources and compare to the ACF of sources for which we have identified

counterparts. Both measurements yielded a clustering amplitude $A \sim 5$, consistent within 1σ. Hence, with regard to the angular clustering, the incompleteness of the SMG identification has little effect. However, it is hard to determine whether it can influence the bias measurements at different redshifts.

An interesting galaxy population to investigate further is that selected by the OIRTC criteria alone, without bright SMG counterparts. There are many more (~3000) submillimetre sources, fainter than 2.7 mJy at wavelength 850 μm (the detection limit of the S2CLS map), that satisfy the OIRTC criteria. A clustering analysis of this population (Chen et al. 2016b) may reduce the size of the error bars of the clustering amplitudes and provide additional constraints on predicted halo masses.

We do not take into account the large-scale cosmic variance in our estimation of our errors, other than the internal uncertainty quantified in our bootstrap analysis. Ideally, we would have multiple independent fields of SMG identifications, which will be soon possible with forthcoming mapping of the COSMOS field with SCUBA-2 in the East Asian Observatory JCMT S2COSMOS survey.

Finally, we return to the issue that submillimetre sources suffer from a blending bias, arising from the blending of multiple counterparts within the SCUBA-2 beam (e.g. Hodge et al. 2013; Karim et al. 2013). Cowley et al. (2016) investigated the clustering evolution of SMGs selected using a combination of the Millennium-style N-body simulation, an updated version of the GALFORM semi-analytic model of galaxy formation (Lacey et al. 2015) and a model for calculating the absorption and re-emission of stellar radiation by dust. They found that galaxies selected by their 850 μm flux densities are hosted by dark matter haloes of mass ~$10^{11.5}$–10^{12} h^{-1} M$_\odot$ over a large redshift range of $0 < z < 4$, consistent with our clustering measurements at $1 < z < 2$. By simulating the submillimetre imaging at 850 μm to match observations with SCUBA-2, [using the method outlined in Cowley et al. (2015)], they demonstrated that confusion between low-resolution sources can artificially boost galaxy bias measurements by a factor of ~2.

To investigate whether this will affect the results presented in this work, we have repeated the analysis of Cowley et al. (2016), using the same redshift bins used in our analysis. In order to assign a redshift to a submillimetre source identified in the simulated imaging, we use the redshift of the galaxy that contributes the largest fraction of the detected single-dish submillimetre flux to the source. Calculating the clustering of the sources in the simulated image within the redshift intervals used here and comparing to the clustering of simulated galaxies in the same redshift interval, we find the blending bias correction reduces from a factor of ~2 to a factor of ~1.2. We attribute this to a reduction in the beam-induced correlations between SMGs at different redshifts as discussed in Cowley et al. (2016). We list these corrections and the corrected galaxy bias values in Table 1, but we have not applied these corrections in the figures. The corrected SMG clustering measurements are lower than (or consistent with, within 1σ errors) those of the star-forming sample, but do not alter our conclusions that SMGs appear to be consistent with other star-forming galaxies at a given epoch.

The precise values of the blending bias correction factors are likely to be model dependent. The model used by Cowley et al. (2015) predicts that close pairs of SMGs are not physically associated and that SMGs singly occupy haloes. There are cases in which blended SMGs are found to be line-of-sight projections (e.g. Zavala et al. 2015), but we note that Simpson et al. (2015b) suggest that the detected overabundance of the faint components of multiple SMGs in ALMA maps implies that a fraction of the

blended SMGs are, on average, physically associated and are not dominated by line-of-sight projection effects. Therefore, the model assumed by Cowley et al. (2015) may lead to larger blending corrections than are necessary. Further work will be required to match model SMG clustering properties with observations, which we defer to a future paper. As an extension, we could input a mock catalogue of galaxies, with known clustering evolution, into the SCUBA-2 pipeline and tune the input clustering until the clustering of output sources matches what is observed. We could therefore predict more accurately the blending bias from this tuning. Alternatively, ALMA will soon reveal which SCUBA-2 sources are blends, allowing for a more precise determination of the true galaxy bias. Based on our current estimates of the likely blending corrections, however, we do not believe these effects will fundamentally alter our conclusions that SMGs reside in haloes comparable to those of star-forming galaxies.

5 CONCLUSIONS

We have used a cross-correlation analysis to study the evolution of SMG clustering and halo masses to $z = 3.5$. This was made possible by analysing the largest sample of SMGs in a single field to date, using a combination of $850\,\mu$m flux densities from the S2CLS, radio imaging and OIRTC criteria [developed by C16] in the UKIDSS UDS. We cross-correlate the SMG sample with a much larger K-selected tracer population, providing significantly improved constraints on halo masses than previously reported. Our main results are summarized as follows.

(i) We performed a cross-correlation analysis of SMGs in the redshift interval $1 < z < 3$, the redshift range of focus in previous studies. We find marginally weaker clustering signals than previously reported, with clustering strength $r_0 = 4.1^{+2.1}_{-2.0}\,h^{-1}$ Mpc. However, within 1σ uncertainty, this is consistent with the measurements derived by earlier smaller-scale studies. We also find that radio-selected SMGs are slightly more strongly clustered, with a clustering strength of $r_0 = 6.8^{+2.7}_{-2.6}\,h^{-1}$ Mpc.

(ii) We analysed the redshift evolution of SMG clustering, deriving halo masses and comparing the measurements with their *UVJ*-selected passive and normal star-forming counterparts. The clustering strengths of SMGs are consistent with the star-forming population and are lower than those of the passive population at the same redshift. This finding holds across all redshifts. We also find tentative evidence of halo downsizing, i.e. SMG activity appears to shift to lower-mass dark matter haloes as the Universe ages. The typical halo masses range from $M_{\mathrm{halo}} > 10^{13}$ M$_\odot$ at redshifts $z > 2.5$, to $M_{\mathrm{halo}} \sim 10^{11}$ M$_\odot$ at redshifts $1 < z < 2$. The diminishing clustering signal indicates that SMG activity gradually moves from high-density environments in the early Universe to low-density environments at later epochs.

(iii) We tested the previously reported link between local massive elliptical galaxies and SMGs, using a dark matter growth rate formalism. We find that $z > 2$ SMGs are consistent with being the progenitors of massive elliptical galaxies found in present-day galaxy clusters. We note, however, that other star-forming galaxies at the same epoch show comparable level of clustering. Overall, we find that SMGs exhibit clustering that is consistent with other star-forming galaxies at a given epoch, with activity shifting from very massive haloes at $z > 2$ to more modest environments at lower redshift.

REFERENCES

Adelberger K. L., Steidel C. C., Pettini M., Shapley A. E., Reddy N. A., Erb D. K., 2005, ApJ, 619, 697
Alexander D. M., Bauer F. E., Chapman S. C., Smail I., Blain A. W., Brandt W. N., Ivison R. J., 2005, ApJ, 632, 736
Assef R. J. et al., 2011, ApJ, 728, 56
Baldry I. K., Balogh M. L., Bower R., Glazebrook K., Nichol R. C., 2004, in Allen R. E., Nanopoulos D. V., Pope C. N., eds, AIP Conf. Proc. Vol. 743, The New Cosmology: Conference on Strings and Cosmology. Am. Inst. Phys., New York, p. 106
Barger A. J., Cowie L. L., Sanders D. B., Fulton E., Taniguchi Y., Sato Y., Kawara K., Okuda H., 1998, Nature, 394, 248
Bell E. F., Wolf C., Meisenheimer K., Rix H.-W., Borch A., Dye S., Kleinheinrich M., McIntosh D. H., 2004, ApJ, 608, 752
Best P. N., Kaiser C. R., Heckman T. M., Kauffmann G., 2006, MNRAS, 368, L67
Blain A. W., Chapman S. C., Smail I., Ivison R., 2004, ApJ, 611, 725
Brammer G. B., van Dokkum P. G., Coppi P., 2008, ApJ, 686, 1503
Brammer G. B. et al., 2009, ApJ, 706, L173
Bruzual G., Charlot S., 2003, MNRAS, 344, 1000
Cen R., 2011, ApJ, 741, 99
Chapman S. C., Blain A. W., Smail I., Ivison R. J., 2005, ApJ, 622, 772
Chapman S. C., Blain A., Ibata R., Ivison R. J., Smail I., Morrison G., 2009, ApJ, 691, 560
Chen C.-C. et al., 2016a, ApJ, 820, 82 (C16)
Chen C.-C. et al., 2016b, preprint (arXiv:1609.00388)
Cooray A. et al., 2010, A&A, 518, L22
Cowley W. I., Lacey C. G., Baugh C. M., Cole S., 2015, MNRAS, 446, 1784
Cowley W. I., Lacey C. G., Baugh C. M., Cole S., 2016, MNRAS, 446, 1621
Croton D. J. et al., 2006, MNRAS, 367, 864
Dannerbauer H. et al., 2014, A&A, 570, A55
Dekel A., Birnboim Y., 2006, MNRAS, 368, 2
Dekel A., Sari R., Ceverino D., 2009, ApJ, 703, 785
Di Matteo T., Springel V., Hernquist L., 2005, Nature, 433, 604
Eales S., Lilly S., Gear W., Dunne L., Bond J. R., Hammer F., Le Fèvre O., Crampton D., 1999, ApJ, 515, 518
Estrada J., Sefusatti E., Frieman J. A., 2009, ApJ, 692, 265
Fakhouri O., Ma C.-P., Boylan-Kolchin M., 2010, MNRAS, 406, 2267
Farrah D. et al., 2006, ApJ, 641, L17
Furusawa H. et al., 2008, ApJS, 176, 1
Furusawa J., Sekiguchi K., Takata T., Furusawa H., Shimasaku K., Simpson C., Akiyama M., 2011, ApJ, 727, 111
Geach J. E. et al., 2013, MNRAS, 432, 53

Geach J. E. et al., 2016, preprint (arXiv:1607.03904)

Hainline L. J., Blain A. W., Smail I., Alexander D. M., Armus L., Chapman S. C., Ivison R. J., 2011, ApJ, 740, 96

Hartley W. G. et al., 2010, MNRAS, 407, 1212

Hartley W. G. et al., 2013, MNRAS, 431, 3045

Hayward C. C., Behroozi P. S., Somerville R. S., Primack J. R., Moreno J., Wechsler R. H., 2013, MNRAS, 434, 2572

Hickox R. C. et al., 2012, MNRAS, 421, 284

Hodge J. A. et al., 2013, ApJ, 768, 91

Holland W. S. et al., 2013, MNRAS, 430, 2513

Hopkins P. F., Hernquist L., Cox T. J., Di Matteo T., Martini P., Robertson B., Springel V., 2005, ApJ, 630, 705

Hopkins P. F., Hernquist L., Cox T. J., Di Matteo T., Robertson B., Springel V., 2006, ApJS, 163, 1

Hughes D. H. et al., 1998, Nature, 394, 241

Ivison R. J. et al., 2002, MNRAS, 337, 1

Ivison R. J. et al., 2005, MNRAS, 364, 1025

Ivison R. J., Papadopoulos P. P., Smail I., Greve T. R., Thomson A. P., Xilouris E. M., Chapman S. C., 2011, MNRAS, 412, 1913

Jullo E. et al., 2012, ApJ, 750, 37

Karim A. et al., 2013, MNRAS, 432, 2

Kennicutt R. C., Jr, 1998, ARA&A, 36, 189

Lacey C. G. et al., 2015, preprint (arXiv:1509.08473)

Landy S. D., Szalay A. S., 1993, ApJ, 412, 64

Lin L. et al., 2016, ApJ, 817, 97

Maddox S. J. et al., 2010, A&A, 518, L11

Magliocchetti M., Porciani C., 2003, MNRAS, 346, 186

Magliocchetti M. et al., 2013, MNRAS, 433, 127

Martig M., Bournaud F., Teyssier R., Dekel A., 2009, ApJ, 707, 250

McCracken H. J. et al., 2015, MNRAS, 449, 901

Meneux B. et al., 2006, A&A, 452, 387

Miller T. B., Hayward C. C., Chapman S. C., Behroozi P. S., 2015, MNRAS, 452, 878

Mitchell-Wynne K. et al., 2012, ApJ, 753, 23

Mo H. J., White S. D. M., 1996, MNRAS, 282, 347

Mo H. J., White S. D. M., 2002, MNRAS, 336, 112

Mortlock A. et al., 2013, MNRAS, 433, 1185

Mortlock A. et al., 2015, MNRAS, 447, 2

Norberg P. et al., 2002, MNRAS, 332, 827

Peebles P. J. E., 1980, The Large-Scale Structure of the Universe. Princeton Univ. Press, Princeton, NJ

Pope A. et al., 2006, MNRAS, 370, 1185

Pozzetti L. et al., 2010, A&A, 523, A13

Prevot M. L., Lequeux J., Prevot L., Maurice E., Rocca-Volmerange B., 1984, A&A, 132, 389

Richards G. T. et al., 2006, AJ, 131, 2766

Roche N., Eales S. A., 1999, MNRAS, 307, 703

Ross A. J., Brunner R. J., 2009, MNRAS, 399, 878

Scoville N. et al., 2007, ApJS, 172, 1

Silk J., Rees M. J., 1998, A&A, 331, L1

Simpson C. et al., 2006, MNRAS, 372, 741

Simpson J. M. et al., 2014, ApJ, 788, 125

Simpson J. M. et al., 2015a, ApJ, 799, 81

Simpson J. M. et al., 2015b, ApJ, 807, 128

Smail I., Ivison R. J., Blain A. W., 1997, ApJ, 490, L5

Smail I. et al., 2014, ApJ, 782, 19

Smith R. E. et al., 2003, MNRAS, 341, 1311

Somerville R. S., Hopkins P. F., Cox T. J., Robertson B. E., Hernquist L., 2008, MNRAS, 391, 481

Steidel C. C., Adelberger K. L., Dickinson M., Giavalisco M., Pettini M., Kellogg M., 1998, ApJ, 492, 428

Strateva I. et al., 2001, AJ, 122, 1861

Swinbank A. M., Chapman S. C., Smail I., Lindner C., Borys C., Blain A. W., Ivison R. J., Lewis G. F., 2006, MNRAS, 371, 465

Tacconi L. J. et al., 2006, ApJ, 640, 228

Tacconi L. J. et al., 2008, ApJ, 680, 246

Targett T. A., Dunlop J. S., McLure R. J., Best P. N., Cirasuolo M., Almaini O., 2011, MNRAS, 412, 295

Thomas D., Maraston C., Schawinski K., Sarzi M., Silk J., 2010, MNRAS, 404, 1775

Toomre A., 1977, in Tinsley B. M., Larson D. Campbell R. B. G., eds, Evolution of Galaxies and Stellar Populations. Yale Univ. Observatory, New Haven, p. 401

Trayford J. W., Theuns T., Bower R. G., Crain R. A., Lagos C. d. P., Schaller M., Schaye J., 2016, preprint (arXiv:1601.07907)

Ueda Y. et al., 2008, ApJS, 179, 124

Umehata H. et al., 2015, ApJ, 815, L8

van Kampen E. et al., 2012, MNRAS, 426, 3455

Wake D. A. et al., 2006, MNRAS, 372, 537

Wake D. A. et al., 2011, ApJ, 728, 46

Webb T. M. et al., 2003, ApJ, 582, 6

Weiß A. et al., 2009, ApJ, 707, 1201

Wild V. et al., 2014, MNRAS, 440, 1880

Williams R. J., Quadri R. F., Franx M., van Dokkum P., Labbé I., 2009, ApJ, 691, 1879

Williams C. C. et al., 2011, ApJ, 733, 92

Yun M. S. et al., 2012, MNRAS, 420, 957

Zavala J. A. et al., 2015, MNRAS, 452, 1140

Zehavi I. et al., 2011, ApJ, 736, 59

This paper has been typeset from a TeX/LaTeX file prepared by the author.